Scientia Iranica, Vol. 14, No. 3, pp 263–272

SCIENTIA IRANICA

Nano-Particle Beam Focusing in Aerodynamic Lenses - An Axisymmetric Model

A. Nikbakht[1], O. Abouali[*] and G. Ahmadi[2]

A computer code for axisymmetric modeling of nano- and micro-particle motions in an aerodynamic particle beam focusing system was developed. The effectiveness of the focusing system, consisting of several lenses, a nozzle and the chamber downstream of the nozzle, was analyzed. The code included an accurate model for the Brownian diffusion of nano-particles in sharply varying pressure fields in the aerodynamic lens system. Assuming an axisymmetric condition, the compressible airflow and thermal field in the lens were evaluated. A Lagrangian particle trajectory analysis was performed, assuming a one-way coupling model. The particle equation of motion used included drag and Brownian forces. Trajectories of different size nano- and micro-particles in an aerodynamic lens were analyzed and the particle beam focusing process was studied. The numerical results for particle velocity, collection efficiency and beam diameter were compared with the experimental data and good agreement was observed. The importance of the accuracy of the Brownian diffusion model, for predicting the focusing performance of aerodynamic lenses in the focusing of nano-particles, was discussed. The simulation results showed that for particle diameters less than 30 nm in air, the Brownian force could significantly affect beam focusing and particle collection efficiency.

INTRODUCTION

Aerodynamic lenses are devices that are used for generating focused particle beams by use of a series of axisymmetric contractions and expansions. Particles in a certain size range passing through a sequence of contractions drift towards the axis and form a narrow beam. Large particles are removed from the stream by inertial impaction on the lens wall, while very small particles follow the flow streamlines and are not focused. Lenses could be designed to generate beams of different diameter of particles of various sizes.

Jayne et al. [1], Zhang et al. [2], Kane and Johnston [3] and Kane et al. [4] described the use of aerodynamic lenses for producing focused aerosol particle beams for online characterization of fine particles. Murphy and Sears [5] reported producing narrow particle beams by expanding an aerosol from atmospheric pressure to low backpressures through a nozzle. Various nozzle types, such as capillary, conically convergent and plate orifice, were used by a number of researchers [6-12]. Highly converging nozzles produce a small beam diameter at a focal point close to the nozzle exit, but produce a highly divergent beam downstream from the nozzle. The beams generated by gradually convergent and capillary nozzles, however, have smaller diameters that can be sustained for longer distances. Mallina et al. [11] showed that, generally, a narrow beam diameter generated by a nozzle is limited to a very small range of particle diameters.

Particle beam focusing can be also achieved by using sheath gas. The sheath gas reduces particle velocity and particle beam diameters. The sheath gas is normally added upstream of the nozzle in the radial direction, which brings the particles toward the axis. As particles get closer to the axis, they experience less radial drag force, which, in turn, results in a narrow focused beam downstream of the nozzle. Dahneke and Cheng [6,7] showed that by using sheath airflow at a rate approximately equal to the inlet flow rate, the particles beam diameter could be reduced by a factor of

1. *Department of Mechanical Engineering, Shiraz University, Shiraz, I.R. Iran.*
*. *Corresponding Author, Department of Mechanical Engineering, Shiraz University, Shiraz, I.R. Iran.*
2. *Department of Mechanical and Aeronautical Engineering, Clarkson University, Potsdam, NY, USA.*

ten. Using the sheath air, however, dilutes the particle concentration and requires an additional air-handling component.

A method for generating focused particle beams that has attracted considerable attention is the use of aerodynamic lenses. These lenses are formed by combining a series of axisymmetric contraction and expansion focusing elements. Liu et al. [13,14] were the first to report computational and experimental studies of aerodynamic lenses. Their study showed that highly collimated particle beams could be produced by the use of aerodynamic lenses. In general, by using a number of aerodynamic lenses in series, particles in a critical size range passing through a contraction drift towards the axis can be collimated to form a focused beam. Liu et al. [13] evaluated the flow field in the lens and the attached nozzle using both incompressible and compressible axisymmetric Navier-Stokes equations and a one-dimensional empirical correlation for flows downstream of the nozzle. They, however, used an isentropic assumption to relate the gas temperature to pressure. The effect of Brownian motion and lift force on the particle beam diameter downstream of the nozzle was also reported in their study.

Jayne et al. [1] developed an aerosol mass spectrometer, which included an aerodynamic lens for generating a focused particle beam. They also studied the performance of the aerodynamic lens using FLUENT^{TM} software. Jayne et al. used a design similar to the inlet system of Liu et al. [13,14], but with a hot surface followed by an electron impact ionization device and a mass spectrometer. These allowed for the real-time analysis of size resolved particle mass and chemical compositions.

Zhang et al. [2] characterized particle beam collimation in a single aerodynamic lens and an individual nozzle using the FLUENT^{TM} software. They found that maximum particle displacement and particle loss occur at a particle Stokes number near unity. The performance characteristics of the lens and the nozzle were found to depend on their geometry, flow Reynolds number and particle Stokes number.

Earlier computational modeling studies of aerodynamic lenses had a number of limitations. In most cases, the influence of the intermediate chamber on the performance was ignored. For example, the work of Jayne et al. [1] was limited to the modeling of flow and particle motions inside aerodynamic lenses up to the nozzle exit. In their computational model, Liu et al. [13] ignored the effects of the impaction of large particles on the lens wall and used an isentropic one-dimensional flow model in the intermediate chamber.

Abouali and Ahmadi [15] studied axisymmetric airflow and particle motions in multistage aerodynamic lenses with the intermediate chamber. In addition to the gas flow field and particle trajectory inside the lens, the gas flow downstream of the nozzle in the intermediate chamber was also analyzed. The suitability of different assumptions for the slip correction was examined and it was shown that the Stokes-Cunningham expression with the variable Cunningham correction factor is reasonably accurate for performance analysis of aerodynamic lenses. It was also shown that the effects of the lift and thermophoresis forces are negligible. The simulation results showed that for particles in the size range of between 50 to 1000 nm, a focusing efficiency of more than 97% could be achieved. The collection efficiency for larger particles, however, decreased somewhat, due to the inertial impaction effects in the focusing elements. For smaller particles (less than 50 nm), the collection efficiency also decreases, due to Brownian motion effects. They used FLUENT^{TM} software and assumed the flow and particle trajectories were axisymmetric. They used a constant slip correction factor in the Brownian force calculation because of the software limitation. So, their results for the diffusion of nano-particles were not quite accurate.

Using FLUENT^{TM}, Zhang et al. [16] presented a numerical model of the flows of gas-particle suspensions through an integrated aerodynamic-lens-nozzle system. They found that the inlet transmission efficiency (η_t) was about unity for particles of intermediate diameters (Dp$\sim$30-500 nm). The transmission efficiency gradually diminished to $\sim$ 40% for large particles (Dp$>$ 2500 nm), because of impact losses on the surface of the first lens. Their result showed that there was a catastrophic reduction of η_t to almost zero for very small particles (Dp $\leq$ 15 nm), because these particles faithfully followed the final gas expansion. Zhang et al. [16] also found that overall particle transmission efficiency can be calculated roughly as the product of the aerodynamic and the purely Brownian efficiencies. For particles of intermediate diameter, Brownian motion was found to be irrelevant, and their results showed that the transmission efficiency was mainly controlled by the lenses. Results for an isolated lens or nozzle were used to provide guidelines for the design of alternative inlets. Like the work of Abouali and Ahmadi's [15], their procedure for Brownian motion simulation was an approximate one.

Wang et al. [17] developed a numerical simulation methodology that was able to accurately characterize the focusing performance of aerodynamic lens systems. They used FLUENT^{TM} software to simulate the gas flow field and particle motion. Particle trajectories were tracked using the Lagrangian approach. Brownian motion of nano-particles was incorporated in their numerical simulations using User's Defined Function (UDF) to augment the software. Their simulations also demonstrated the ability of aerodynamic lenses to focus sub-30 nm spherical unit density particles.

To avoid the limitations of commercial software, in the present study, a computer code, for analyzing the axisymmetric particle motions in multistage aerodynamic lenses with the intermediate chamber, was developed. The flow field was simulated using FLUENT^{TM} software and particle trajectories inside the lens, through the outlet nozzle and in the intermediate chamber downstream of the nozzle, were analyzed, using the developed code. The effectiveness of an aerodynamic lens for particle beam focusing was examined.

MODEL DESCRIPTION

The aerodynamic lens system used by Liu et al. [13,14] consists of a multistage focusing lens, an outlet nozzle, an intermediate chamber and a detection chamber. In this paper, the aerodynamic lens system, including the intermediate chamber shown in Figure 1, is computationally modeled.

The diameter of the lens tube is 10 mm and adjacent focusing elements are located 50 mm apart. The contraction diameters of the five lenses that are used in the analysis are 5.0, 4.5, 4.0, 3.75 and 3.5 mm, respectively. The first, the third and the fifth lenses are short capillaries with a length of 10 millimeters and the second and the fourth lenses are thin-plate orifices. At the end of the five focusing elements, the gas passes through a nozzle with a diameter of 6 mm. In the experimental work of Liu et al. [14], the flow expands in the aerodynamic focusing elements and the nozzle into a low-pressure intermediate chamber, which is kept at about 0.07 mmHg (9.3 Pa). A vacuum pump is attached to the intermediate chamber to remove a significant amount of gas from the stream. Focused particles and a small amount of gas pass through a skimmer into a very low-pressure detection chamber. The detection chamber is kept at a pressure of about 0.0007 mmHg (0.093 Pa). Particles are captured on a plate at the end of the detection chamber.

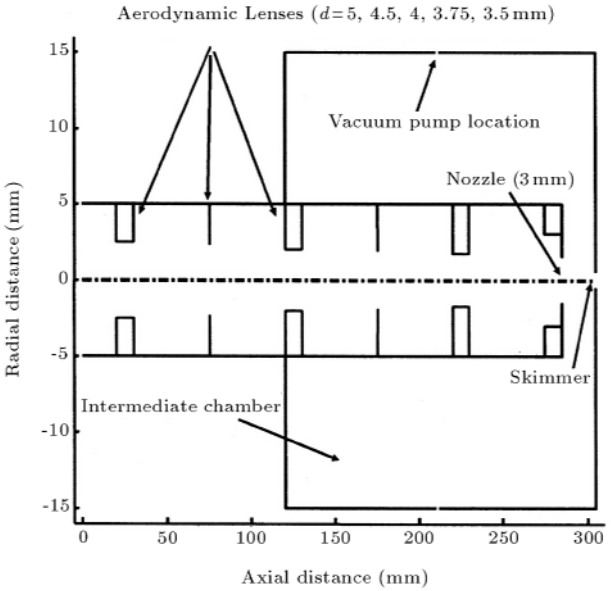

Figure 1. Schematics of the aerodynamic lens system.

The mean free path of the gas in the detection chamber is of the order of chamber size; thus, for this chamber, the continuum flow assumption is not valid. The gas flow in the intermediate chamber downstream of the nozzle, with $\lambda/L = 0.1$, however, may be treated as being in the continuum regime. The flow in the lens and the nozzle is axisymmetric; the flow in the intermediate chamber, however, is not axisymmetric, due to the presence of the vacuum pump exhaust. Nevertheless, as a first approximation, the problem is treated as being axisymmetric.

GOVERNING EQUATIONS

In an aerodynamic lens, the gas-particle flow is dilute and a one-way interaction model can be used. In this model, the particles are transported by the airflow, but, the particle concentration is too low to affect the gas flow. Under this condition, the airflow field can first be evaluated and then be used for evaluation of the particle trajectories. Here, the compressible viscous airflow conditions in the aerodynamic lens are evaluated. Details of the governing equations for an axisymmetric flow condition are given in the FLUENT^{TM} Users' Guide [18].

The Lagrangian equation of particle motion is given as:

$$\frac{d\mathbf{V}_p}{dt} = \mathbf{F}_D + \mathbf{F}_B + g(\rho_p \quad \rho)/\rho_p, \tag{1}$$

$$\frac{dx_p}{dt} = \mathbf{V}_p, \tag{2}$$

where $\mathbf{V}_p$ is the particle velocity vector, $\mathbf{F}_D$ is the drag force per unit mass, $\mathbf{F}_B$ is the Brownian force per unit mass, g is the acceleration of gravity, ρ is the gas density, ρ_p is the particle density and x_p is the particle position vector. Note that the flow is in a laminar regime and the particles are assumed to be spherical.

Drag Force

The expression for the Stokes drag force per unit mass, including the Cunningham correction, is given by:

$$\mathbf{F}_D = \frac{3\mu C_D \mathrm{Re}}{4\rho_p D_p^2 C_c}(\mathbf{V} \quad \mathbf{V}_p), \tag{3}$$

where $\mathbf{V}$ is the fluid velocity vector, D_p is particle diameter, μ is the coefficient of viscosity and C_c is the

Cunningham correction factor, given as:

$$C_c = 1 + \frac{2\lambda}{D_p}\left[1.257 + 0.4\exp\left(\quad 1.1\left(\frac{D_p}{2\lambda}\right)\right)\right], \quad (4)$$

and Re, the particle Reynolds number, is defined as:

$$\mathrm{Re} = \frac{|\mathbf{V} \quad \mathbf{V}_p| D_p}{\nu}, \quad (5)$$

where ν is the kinematic viscosity of the gas. In Equation 3, the drag coefficient, C_D, which accounts for the Reynolds number correction to the Stokes drag, is given as:

$$C_D = \frac{24}{\mathrm{Re}}(1 + 0.15\mathrm{Re}^{0.687}). \quad (6)$$

Note that the nonlinear corrections are expected to be significant only for larger particles with appreciable slip velocity. For nano-particles with small slip velocity, Re is very small and the second term in Equation 6 will be negligible.

For nano-particles in aerodynamic lenses, the Knudsen number, $\mathrm{Kn} = 2\lambda/D_p$, varies in the range of 50-10^6, which covers the range of transition to a free molecular regime. This is due to the tremendous range of variation of pressure in the lens. For high values of Knudsen numbers, the Cunningham correction factor given by Equation 4 may be approximated as $C_c \approx 1.657\,\mathrm{Kn}$. Neglecting the nonlinear Reynolds number correction in Equation 6, Equation 3 reduces to the expression for the free molecular drag (per unit mass) for the case of the diffuse reflection of air molecules from the particle surface (that is, $\mathbf{F}_D = \frac{3\pi\mu d_p^2(\mathbf{V} \quad \mathbf{V}_p)}{3.32\lambda}$, which is the drag force for the free molecular flows).

In Equation 4, the Cunningham correction factor depends on the gas mean free path. There is a significant change in the gas mean free path in the aerodynamic lens, due to the large variations in gas pressure. Therefore, the Cunningham correction factor must be calculated using the correct gas mean free path along particle trajectories for an accurate simulation of the drag and Brownian forces. The mean free path of air is given as [19]:

$$\lambda(\mu m) = \frac{kT}{\sqrt{2}\pi d_m^2 P} = \frac{23.1T}{P}. \quad (7)$$

In Equation 7, d_m, k, P and T, respectively, are the gas molecule diameter (0.361 nm), the Boltzmann constant, gas pressure (Pascal) and gas temperature (Kelvin).

Brownian Force

When a small particle is suspended in a fluid, it is subjected to the imbalanced random impacts of the gas molecules. This causes the nano-particles to move in an erratic path, which is known as Brownian motion. A Gaussian white noise stochastic process can model the random impacts of the molecules. White noise is a zero mean Gaussian random process with a constant power spectrum, given by:

$$S_{nn} = \frac{2kT\beta}{\pi m}, \quad (8)$$

where $k = 1.38.10^{\ -23}$ J/K is the Boltzmann constant. The procedure suggested by Ounis and Ahmadi [20] and Li and Ahmadi [21] for simulating Brownian motion was used in the computer code developed in this study.

To start the process, a time step, Δt, is selected. (The time step should be much smaller than the particle relaxation time.) Then, a pair of uniform random numbers, U_i (between 0 and 1), are generated and are transformed to a pair of unit variance zero mean Gaussian random numbers. This is done using the following transformations:

$$G_1 = \sqrt{\quad 2\ln U_1}\cos(2\pi U_2), \quad (9)$$

$$G_2 = \sqrt{\quad 2\ln U_1}\sin(2\pi U_2). \quad (10)$$

The amplitude of the Brownian force per unit mass in direction i at each time step is then evaluated by:

$$F_{bi} = G_i\sqrt{\frac{\pi S_{nn}}{\Delta t}}, \quad (11)$$

where S_{nn} is given by Equation 8. The entire generated sample of the Brownian force is then shifted by $U\Delta t$, where U is a uniform random number between zero and one.

Variable Cunningham Correction

As noted before, a constant Cunningham correction factor can be used in the particle analysis module of the FLUENT code. The Cunningham slip correction factor depends on the Knudsen number or the gas mean free path. The gas mean free path is a function of the gas pressure (density). When a constant correction factor is used, the mean free path, as a function of gas pressure at an appropriate point of the flow, needs to be evaluated. Mallina et al. [22] used the nozzle exit pressure for evaluating the correction factor, in connection with their study of supersonic impactors. Tafreshi et al. [23] and Zhang et al. [2] used an average pressure for evaluating a constant Cunningham correction factor for their focusing studies. In cases where the pressure variation is large, the range of variation of the Cunningham correction factor also becomes large and a constant correction factor for the entire field

is no longer adequate. Since FLUENT software, by default, allows only for a fixed Cunningham correction factor, Abouali and Ahmadi [15,24] and Wang et al. [17] developed "users' defined subroutines" to include the effect of variation of the mean free path in the analysis. Considering a variable slip factor in the Brownian force is another important requirement of the Diffusion modeling of the nano-particles. Here, to avoid the limitations of commercial software, a computer code was developed as post processing for the FLUENT code for particle trajectory analysis in regions with a high level of pressure variation. The new computational model incorporates accurate expressions for the drag force and the intensity of Brownian excitation, with appropriate variations of the gas mean free path. Thus, the code is most suitable for analyzing the particle focusing in aerodynamic lenses where significant variations of the pressure field are encountered.

Numerical Method

Particle trajectories and velocities were computed by numerically integrating the equation of motion of the particle given by Equation 1, which includes inertia, gravity, drag and random Brownian forces. A forward Euler scheme was used for integrating the particle equation of motion, that is:

$$\frac{\mathbf{V}_p^{n+1} \quad \mathbf{V}_p^n}{\Delta t} = \mathbf{F}_b + \frac{3\mu C_D \mathrm{Re}}{4\rho_p D_p^2 C_c}(\mathbf{V}^n \quad \mathbf{V}_p^{n+1}), \qquad (12)$$

where n represents the iteration number. Note that gravitational effects that are negligible for nano-particles are neglected in Equation 12. The positions of the particle are then given as:

$$\frac{\mathbf{x}_p^{n+1} \quad \mathbf{x}_p^n}{\Delta t} = \mathbf{V}_p^n. \qquad (13)$$

Equations 12 and 13 are solved to predict the particle trajectories. Note that the integration time step must be at least one order of magnitude less than the particle relaxation time, $\tau = \frac{mC_c}{3\pi\mu d_p}$.

RESULTS

For the experimental conditions of Liu et al. [14], the flow fields in a class of aerodynamic lenses are simulated using a computational modeling approach. Liu et al. [14] used two different geometries in their experiments, which are studied in this section. In the first case, where the skimmer diameter was 7mm, the distance between the nozzle and the skimmer was 10 mm (henceforth to be called the larger skimmer). In the second case, the skimmer diameter was 1 mm and the distance between the nozzle and the skimmer was 20 mm. This case will be referred to as the small skimmer lens. The airflow and particle beam focusing in aerodynamic lenses, with a combination of the focusing element, their attached outlet nozzles and the intermediate chamber, are studied.

Computational Grid and Boundary Conditions

A computational grid of 50960 was used for simulating gas flow in the axially symmetric aerodynamic lens, including the intermediate chamber. The grid size was selected after a number of grid independency tests to make sure that the grid was sufficiently refined, so that the solution would not change with further grid refinement. The grid is more refined near the walls and in the supersonic free jet region downstream of the nozzle.

A mass flow rate boundary condition at the aerodynamic lens inlet was used. Fixed pressure boundary conditions were imposed at the skimmer and at the exit to the vacuum pump. Examination of the numerical results shows that, for the large skimmer (with a diameter of 7 mm), 73% of the mass flow rate passes through the skimmer. For the small skimmer (with a diameter of 1 mm), however, most of the flow is sucked up by the vacuum pump and only 1% of the flow exits through the skimmer.

In the experimental study of Liu et al. [14], the pressure upstream of the lenses was about 300 Pa, the pressure in the intermediate chamber was 9.3 Pa and the pressure in the detection chamber was 0.093 Pa (near vacuum). The flow in the detection chamber was clearly in a non-continuum regime because of the large Knudson number (large gas mean free path), with $K_n = 2\lambda/L \sim 20$. The flow in the intermediate chamber, with $\lambda/L \sim 0.1$, however, may be assumed to be approximately in the continuum regime.

Figure 2 shows the airflow velocity and pressure variations along the axis of the aerodynamic lens system for the small skimmer case. The pressure field drops rapidly at the lens orifice and the nozzle contraction sections and in the supersonic free jet downstream of the nozzle. As expected, the air velocity shows sharp peaks at those sections when the pressure drops. The velocities of 10, 30 and 50 nm particles injected at the inlet axis are shown in Figure 2 for comparison. The particles velocity is nearly equal to airflow velocity inside the lens, but they differ from the gas velocity in the supersonic free jet region downstream of the nozzle. The differences are larger for larger particle diameters. This observation shows that, inside the lens, the drag force is sufficiently high to make the particles move very close to the air velocity; in the downstream of the nozzle where the pressure is very low, the drag on the particles is also low and the inertial forces, even for nano-particles, are sufficient to make the particles lag the airflow.

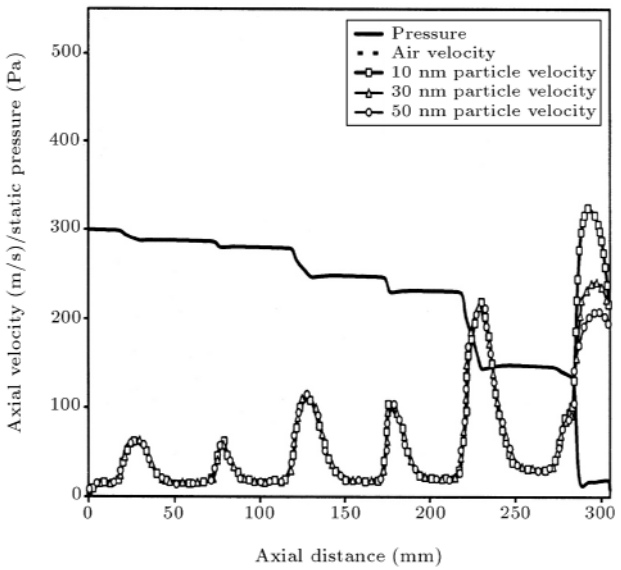

Figure 2. Axial velocity, static pressure and particle velocities along the axis of the aerodynamic lens system for the small skimmer case.

Figure 3 shows similar results for the large skimmer lens with a similar trend of variations. The airflow velocity and particle velocities in the lens are nearly the same as those in the small skimmer case, as shown in Figure 2. The airflow and particle velocities in the supersonic free jet region and the region near the skimmer are, however, different from the small skimmer case. This is because of the differences in the pressure field and the corresponding effect on the drag force on the particles. It should be noted here that the Brownian motion caused the 10 nm particle injected at the axis to disperse away from the axis, so that some fluctuations are seen in its velocity (Figure 3).

Liu et al. [14] measured particle velocity far downstream of the nozzle in the detection chamber at a distance of 200 mm for a large skimmer case. Figure 4 compares the present simulation results for particle velocity with the experimental data. Since the particle velocities in the nearly vacuum condition in the detection chamber remain roughly unchanged, in Figure 4, the simulated particle velocities at the skimmer (which is the inlet of the detection chamber) are shown. Figure 4 shows that the model predictions are in good agreement with the experimental data. To emphasize the importance of accurate evaluation of the slip correction factor, the model prediction results for a constant Cunningham factor, based on the nozzle upstream properties, are also shown in this figure. Figure 4 shows that the use of constant slip correction led to large differences in particle velocities, compared to experimental data.

Figure 5 compares the predicted particle beam diameter with the experimental data of Liu et al. [14] for large skimmer cases. The measurement of the beam diameter was done in the detection chamber, 430 mm downstream of the nozzle. Since, for nano-particles, the beam diameter varies randomly, due to Brownian motion, and some particles disperse to some distances from the axis, here, the beam diameter was estimated to include 90 percent of the particles which are nearest to the axis. For comparison with the experimental data in the detection chamber, the particle beam diameter was evaluated at the skimmer of the intermediate chamber 10 mm downstream of the nozzle and was extrapolated using a divergent angle to the location

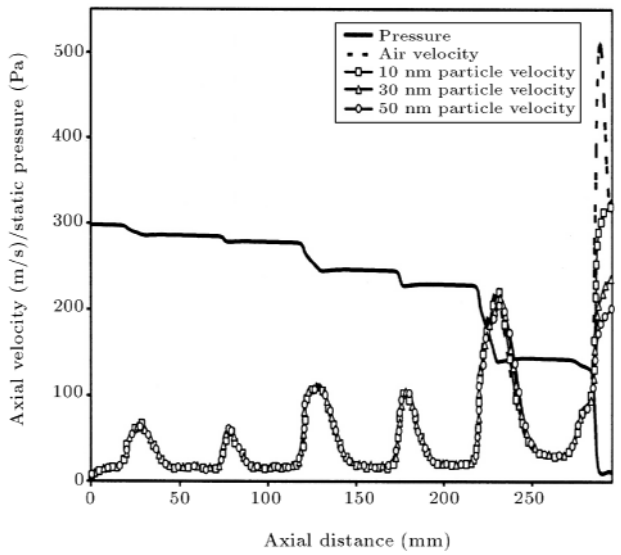

Figure 3. Axial velocity, static pressure and particle velocities along the axis of the aerodynamic lens system for the large skimmer case.

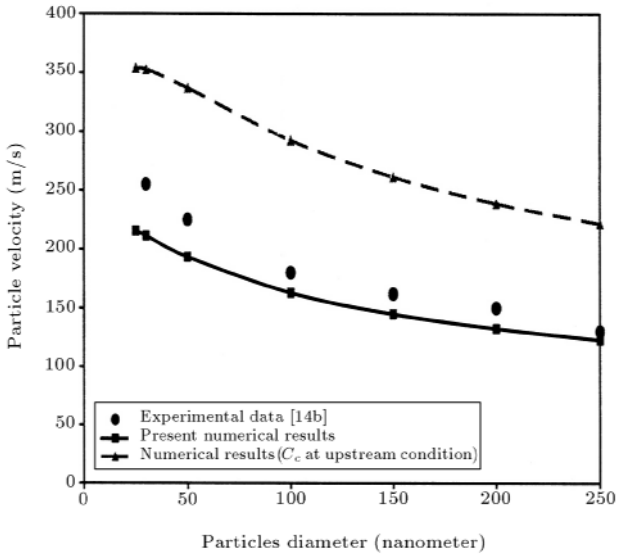

Figure 4. Comparison of the predicted particle velocities with the experimental data of Liu et al. [14] for different particle diameters.

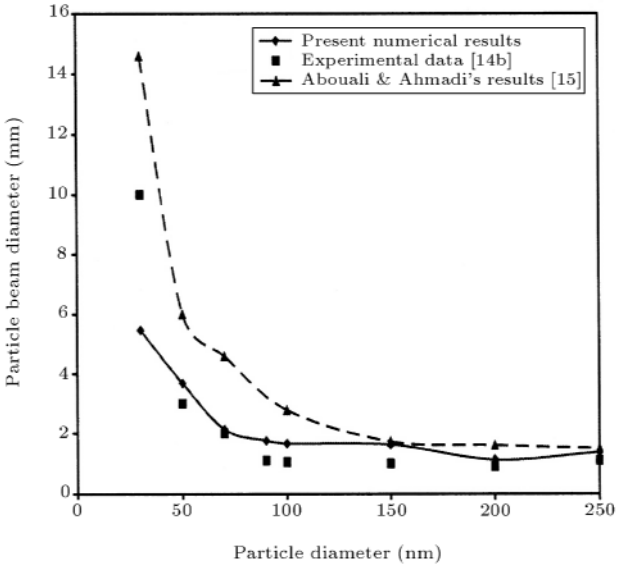

Figure 5. Comparison of the predicted beam diameters with the experimental data of Liu et al. [14] for different particle diameters.

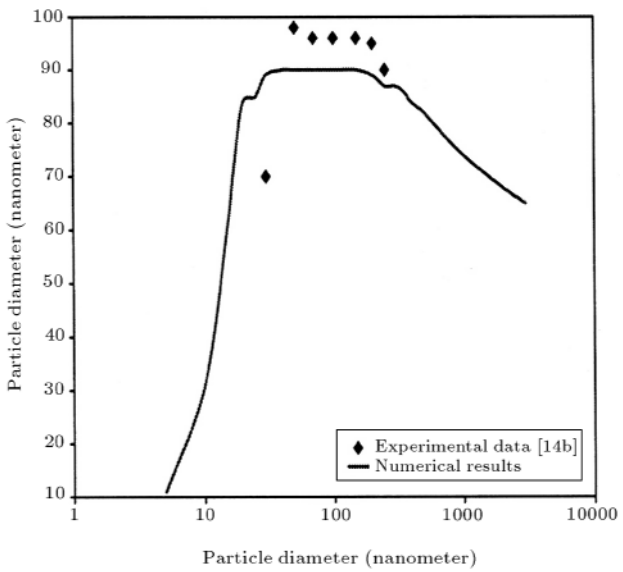

Figure 6. Comparison of the predicted collection efficiencies of the aerodynamic lens and the nozzle system with the experimental data of Liu et al. [14] for different particle diameters.

where it had been measured experimentally. Figure 5 shows that the model predictions for the beam diameter are in good agreement with the experimental data of Liu et al. [14]. The model predictions of Abouali & Ahmadi [15], which were obtained by the use of Brownian excitation with a constant slip correction factor and by the use of the FLUENT software, are also shown in this figure for comparison. It is seen that the present model predictions with the variable Cunningham correction factor improved the agreement with the data significantly.

Figure 6 shows the predicted collection efficiency of the aerodynamic lens and the nozzle system. Here, the collection efficiency is defined as the ratio of the collected particles in the detection chamber to the number of particles entering the aerodynamic lens system. The experimental data of Liu et al. [14], in the case of an intermediate chamber with a small skimmer, is also shown in this figure for comparison. The model prediction appears to be in good agreement with the experimental data and shows that there is an optimal particle size range for collimation. The decreasing trend of the collection efficiency for particles larger than the optimal size range is due to the impaction of particles on the lens wall. Similarly, for particles smaller than the optimal size range, the Brownian motion increases the dispersion and causes the particles to be trapped on the chamber wall or to be carried by the gas into the outlet connected to the vacuum pump.

Figures 7 and 8 show the sample particle trajectories in the aerodynamic lens system for particle diameters of 1, 3, 6, 10, 30 and 50 nm, with and without inclusion of the Brownian force. Here, the case of a lens with a small skimmer is considered and, for illustrative purposes only, 10 particles are injected at the inlet. It is seen that for particles of 1 nm diameter, all are deposited on the walls, due to the Brownian diffusion, but, without Brownian diffusion, all particles get through the nozzle and exit to the suction pump. For particles of 3 nm diameter, some reach the nozzle exit, although they are highly dispersed because of Brownian motion, with many depositing on the focusing elements or chamber walls. Diffusion appears to be still significant for 6 and 10 nm particles, but particles stay closer to the lens axis with none being lost to the suction pump. For particles of 30 nm and greater, no significant differences can be seen between the cases with and without Brownian motion. Figure 8, shows that particles of 30 and 50 nm are highly focused near the axis and exit from the skimmer to the detection chamber. This figure shows that the Brownian effects reduce the effectiveness of the aerodynamic beam focusing for particles of the order of 10 nm or smaller, for the range of pressure conditions considered in the present study.

Figure 9 compares particle trajectories, using a constant and variable slip correction factor in the spectral density of the white noise used for modeling the Brownian motion. This figure shows the importance of accurate modeling of the Brownian diffusion for nano-particles in an aerodynamic lens system. It is seen that using a constant Cunningham correction factor for intensity of Brownian excitation leads to completely different results for the diffusion of nano-particles.

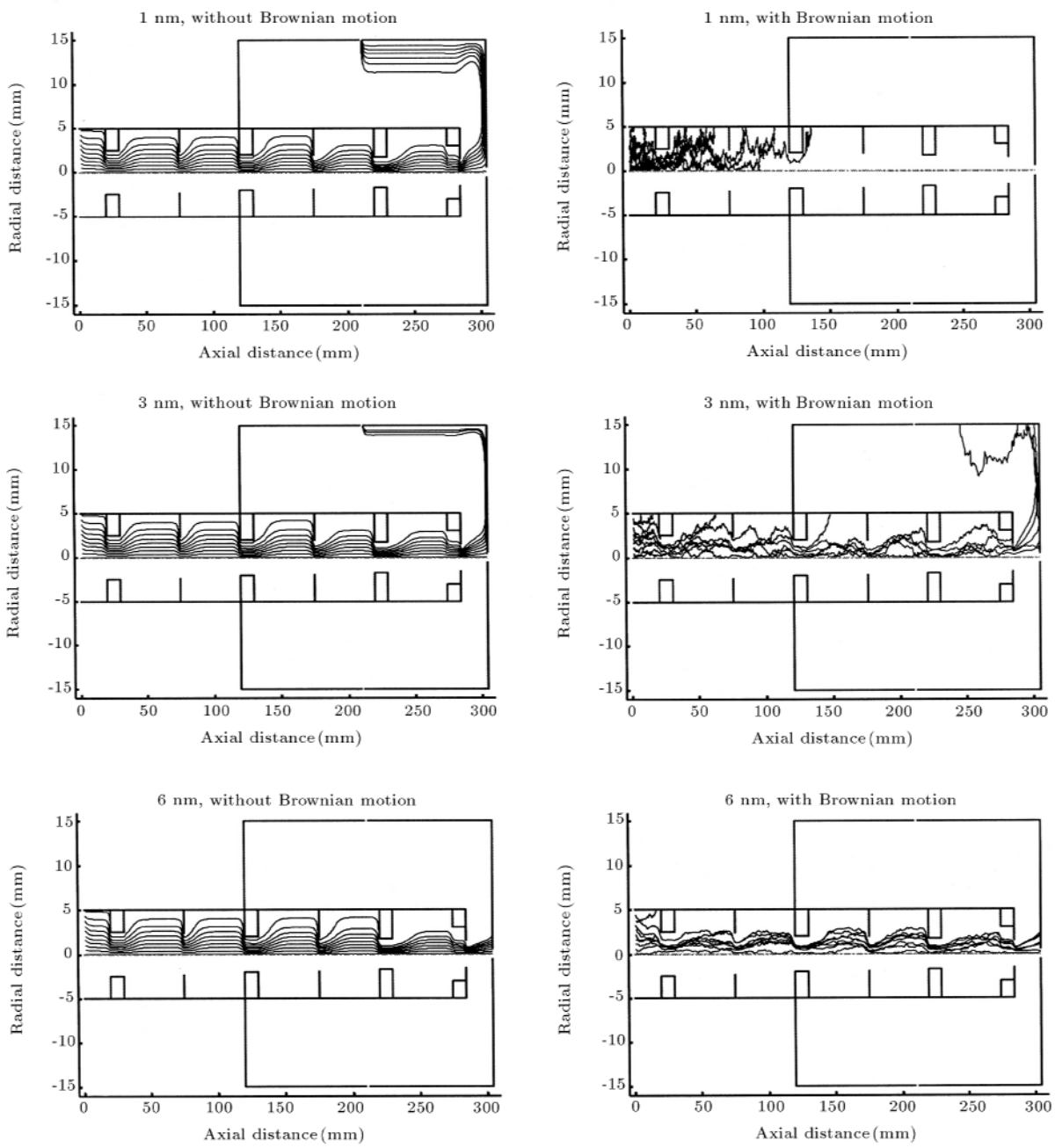

Figure 7. Sample trajectories through the aerodynamic lens including focusing elements, nozzle and intermediate chamber with and without Brownian motion for 1, 3 and 6 nm particles.

CONCLUSIONS

In the present study, airflow and particle motions in a multistage aerodynamic lens with an end nozzle and intermediate chamber, were studied. In addition to the gas flow field and particle trajectories inside the lens, the gas flow and particle motion downstream of the nozzle in the intermediate chamber were also analyzed. A computer code was developed to solve the governing equation of the particles motion, including the Brownian and drag force. It was found that the model predictions for particle velocity, beam diameter and collection efficiency were in favorable agreement with the experimental data of Liu et al. [14]. The simulation results showed that, for particles in the size range of between 30 to 200 nm, a collection efficiency of more than 90% can be achieved. The collection efficiency for larger particles, however, decreased somewhat, due to the inertial impaction effects in the focusing elements. For smaller particles (less than 30 nm), the collection efficiency also decreased, due to Brownian motion effects.

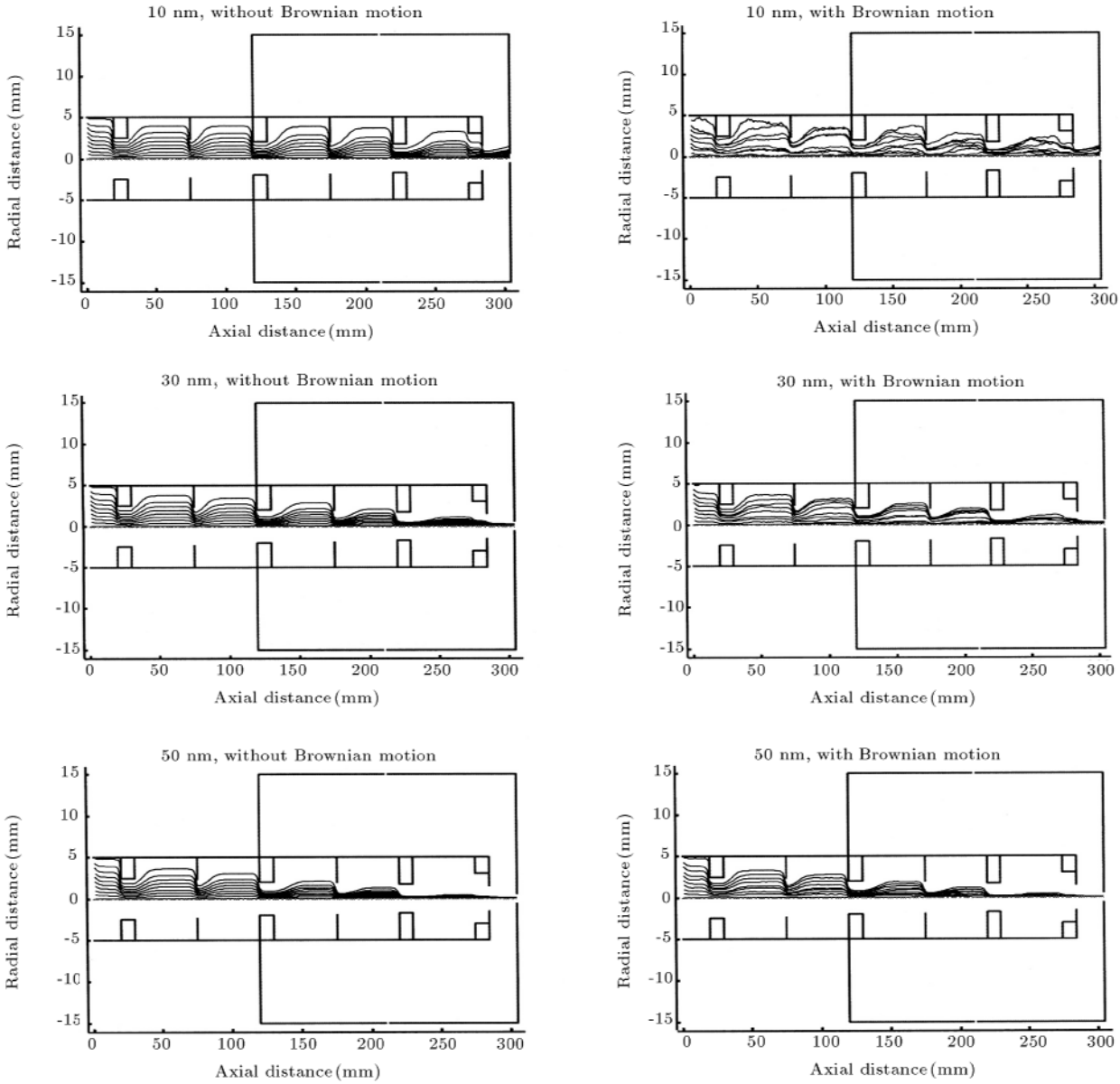

Figure 8. Sample trajectories through the aerodynamic lens including focusing elements, nozzle and intermediate chamber with and without Brownian motion for 10, 30 and 50 nm particles.

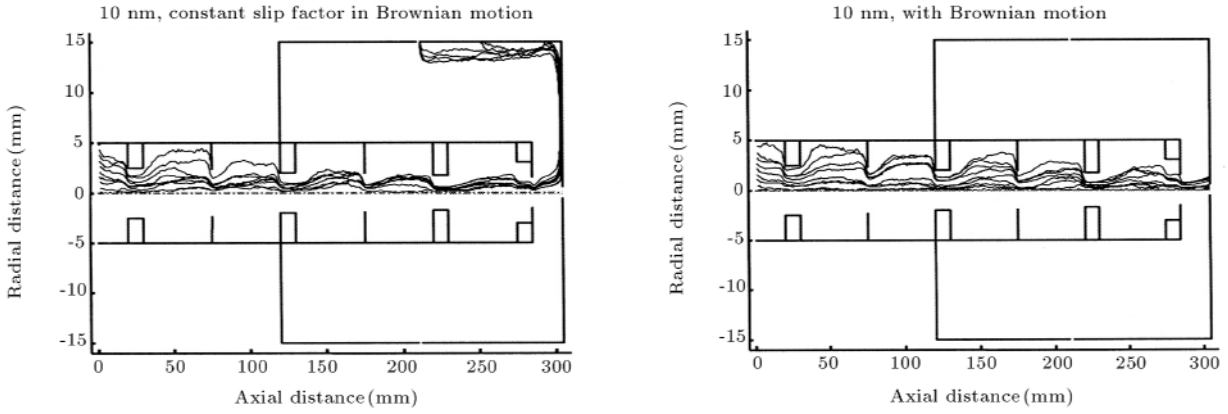

Figure 9. Comparison of particles trajectories for constant and variable slip correction factors.

REFERENCES

1. Jayne, J.T., Leard, D.L., Zhang, X., Davidovits, P., Smith, K.A., Kolb, C.E. and Worsnop, D.R. "Development of an aerosol mass spectrometer for size and composition analysis of submicron particles", *Aerosol Sci. Technol.*, **33**, pp 49-70 (2000).
2. Zhang, X., Smith, K.A., Worsnop, D.R., Jimenez, J., Jayne, J.T. and Kolb, C.E. "A numerical characterization of particle beam collimation by an aerodynamic lens-nozzle system: Part I. An individual lens or nozzle", *Aerosol Sci. Technol.*, **36**, pp 617-631 (2002).
3. Kane, D.B. and Johnston, M.V. "Size and composition biases on the detection of individual ultrafine particles by aerosol mass spectrometry", *Environmental Sci. Technol.*, **34**, pp 4887-4893 (2000).
4. Kane, D.B., Oktem, B. and Johnston, M.V. "Nanoparticle detection by aerosol mass spectrometry", *Aerosol Sci. Technol.*, **34**, pp 520-527 (2001).
5. Murphy, W.K. and Sears, G.W. "Production of particles beams", *J. Appl. Phys.*, **35**, pp 1986-1987 (1964).
6. Dahneke, B.E. and Cheng, Y.S. "Properties of continuum source particle beam. I. Calculation method and results", *J. Aerosol Sci.*, **10**, pp 257-274 (1979a).
7. Dahneke, B.E. and Cheng, Y.S. "Properties of continuum source particle beam. II. Beam generated in capillary expansion", *J. Aerosol Sci.*, **10**, pp 257-274 (1979b).
8. Estes, T.J., Vilker, V.L. and Friendlander, S.K. "Characteristics of a capillary generated particle beam", *J. Colloid Interface Sci*, **93**, pp 84-94 (1983).
9. Fernandez de la Mora, J. and Riesco-Chueca, P. "Aerodynamic focusing of particles in a carrier gas", *J. Fluid. Mech.*, **195**, pp 1-21 (1988).
10. Israel, G.W. and Freidlander, S.K. "High speed beams of small particles", *J. Colloid Interface Sci.*, **24**, pp 330-337 (1967).
11. Mallina, R.V., Wexler, A.S. and Johnson, M.V. "High speed particle beam generation: Simple focusing mechanisms", *J. Aerosol Sci.*, **30**, pp 719-738 (1999).
12. Middha, P. and Wexler, A.S. "Particle focusing characteristics of sonic jet", *Aerosol Sci. Technol.*, **37**, pp 907-915 (2003).
13. Liu, P., Ziemann, P.L., Kitt elson, D.B. and McMurry, P.H. "Generating particle beams of controlled dimensions and divergence: I. Theory of particle motion in aerodynamic lenses and nozzle expansions", *Aerosol Sci. Technol.*, **22**, pp 293-313 (1995a).
14. Liu, P., Ziemann, P.L., Kitt elson, D.B. and McMurry, P.H. "Generating particle beams of controlled dimensions and divergence: II. Experimental evaluation of particle motion in aerodynamic lenses and nozzle expansions", *Aerosol Sci. Technol.*, **22**, pp 314-324 (1995b).
15. Abouali, O. and Ahmadi, G. "Bow shock effect on particle transport and deposition in a hypersonic impactor", *ASME Fluid Engineering Summer Conference*, Honolulu, Hawaii, July 7-11 (2003).
16. Zhang, X., Smith, K.A., Worsnop, D.R., Jimenez, J., Jayne, J.T., Kolb, C.E., Morris, J. and Davidovits, P. "Numerical characterization of particle beam collimation: Part II, Integrated aerodynamic lens-nozzle system", *Aerosol Sci. Technol.*, **38**, pp 619-638 (2004).
17. Wang, X., Gidwani, A., Girshick, S.L. and McMurry, P.H. "Aerodynamic focusing of nanoparticles: II. Numerical simulation of particle motion through aerodynamic lenses", *Aerosol Sci. Technol.*, **39**, pp 624-636 (2005).
18. *FLUENT User Guide (Version 6)*, Fluent Inc., Lebanon, NH, USA.
19. Hering, S.V., Friedlander, S.K., Collins, J.J. and Richards, L.W. "Design and evaluation of a new low-pressure impactor", *Envir. Sci. Technol.*, **13**(2), pp 184-188 (1979).
20. Ounis, H., Ahmadi, G. and McLaughlin, J.B. "Numerical simulation of Brownian particle diffusion in a turbulent channel flow", In *Advances in Micromechanics of Granular Materials*, Eds. by H.H. Shen et al., Elsevier, Amsterdam, pp 433-442 (1992).
21. Li, A. and Ahmadi, G. "Deposition of aerosols on surfaces in a turbulent channel flow", *Intl J. Engng Sci.*, **31**, pp 435-445 (1993).
22. Mallina, R.V., Wexler, A.S., Rhoads, K.P. and Johnson, M.V. "High speed particle beam generation: A dynamic focusing mechanism for selecting ultrafine particles", *Aerosol Sci. Technol.*, **33**, pp 87-104 (2000).
23. Tafreshi, H.V., Benedek, G., Piseri, G., Vinati, S., Barborini, E. and Milani, P. "A simple nozzle configuration for the production of low divergence supersonic cluster beam by aerodynamic focusing", *Aerosol Sci. Technol.*, **36**, p 593 (2002).
24. Abouali, O. and Ahmadi, G. "A model for supersonic and hypersonic impactors for nanoparticles", *Journal of Nanoparticles, J. Nanoparticle Research*, **7**, pp 75-88 (2005).